Stellar feedback and triggered star formation in the prototypical bubble RCW 120

Matteo Luisi, Loren D. Anderson, Nicola Schneider, Robert Simon, Slawa Kabanovic, Rolf Gusten, Annie Zavagno, Patrick S. Broos, Christof Buchbender, Cristian Guevara, et al.

ASTRONOMY

Stellar feedback and triggered star formation in the prototypical bubble RCW 120

Matteo Luisi[1,2]*, Loren D. Anderson[1,2,3], Nicola Schneider[4], Robert Simon[4], Slawa Kabanovic[4], Rolf Güsten[5], Annie Zavagno[6], Patrick S. Broos[7], Christof Buchbender[4], Cristian Guevara[4], Karl Jacobs[4], Matthias Justen[4], Bernd Klein[5], Dylan Linville[1,2], Markus Röllig[4], Delphine Russeil[6], Jürgen Stutzki[4], Maitraiyee Tiwari[5,8], Leisa K. Townsley[7], Alexander G. G. M. Tielens[8,9]

Radiative and mechanical feedback of massive stars regulates star formation and galaxy evolution. Positive feedback triggers the creation of new stars by collecting dense shells of gas, while negative feedback disrupts star formation by shredding molecular clouds. Although key to understanding star formation, their relative importance is unknown. Here, we report velocity-resolved observations from the SOFIA (Stratospheric Observatory for Infrared Astronomy) legacy program FEEDBACK of the massive star-forming region RCW 120 in the [CII] 1.9-THz fine-structure line, revealing a gas shell expanding at 15 km/s. Complementary APEX (Atacama Pathfinder Experiment) CO J = 3-2 345-GHz observations exhibit a ring structure of molecular gas, fragmented into clumps that are actively forming stars. Our observations demonstrate that triggered star formation can occur on much shorter time scales than hitherto thought (<0.15 million years), suggesting that positive feedback operates on short time periods.

INTRODUCTION

Radiative and mechanical feedback by massive stars on their nascent clouds is thought to play a key role in limiting the star formation efficiency of molecular clouds ("negative feedback"), and this controls the evolution of galaxies (*1*–*3*). Photo-ionization by ultraviolet photons will set up evaporative ionized gas flows, removing material from these clouds (*4*). Massive stars also have powerful winds that efficiently remove material from molecular clouds (*5*–*8*). Both processes often create a bubble geometry, with the formation of a compressed shell in which new stars form ("positive feedback") when the gas becomes gravitationally unstable (*9*, *10*). While observations reveal that bubbles are common in regions of massive star formation (*11*, *12*), the relative importance of the effects of positive and negative feedback from high-mass stars on future star formation is unknown.

RCW 120 is a nearby (~1.7 kpc) HII region with a physical diameter of ~4.5 pc (*13*). The region is ionized by a single O8V star, CD −38°11636 (LSS 3959) (*14*), and is known for its near-perfect circular symmetry at mid-infrared (IR) wavelengths (*15*, *16*). The expansion of the HII region has presumably led to the formation of massive clumps along the boundary that are the sites of recent and ongoing star formation (*17*–*20*). RCW 120 is considered to be the prototypical triggered star formation source given the simple region morphology and the abundance of ongoing star formation around its edges. Because of its vicinity and its importance in the context of triggered star formation, RCW 120 has been studied extensively through observations (*15*, *16*, *18*, *19*, *21*–*24*) and simulations (*25*–*29*).

[1]Department of Physics and Astronomy, West Virginia University, Morgantown, WV 26506, USA. [2]Center for Gravitational Waves and Cosmology, West Virginia University, Chestnut Ridge Research Building, Morgantown, WV 26505, USA. [3]Adjunct Astronomer at the Green Bank Observatory, P.O. Box 2, Green Bank, WV 24944, USA. [4]I. Physik. Institut, University of Cologne, Zülpicher Str. 77, 50937 Cologne, Germany. [5]Max-Planck Institut für Radioastronomie, Auf dem Hügel 69, 53121 Bonn, Germany. [6]Aix Marseille Université, CNRS, CNES, LAM, Marseille, France. [7]Department of Astronomy and Astrophysics, 525 Davey Laboratory, Pennsylvania State University, University Park, PA 16802, USA. [8]Department of Astronomy, University of Maryland, College Park, MD 20742, USA. [9]Leiden Observatory, Leiden University, PO Box 9513, 2300 RA Leiden, Netherlands.
*Corresponding author. Email: maluisi@mix.wvu.edu

RESULTS AND DISCUSSION

Observations of RCW 120

We have used the upGREAT (German Receiver for Astronomy at Terahertz) instrument on the Stratospheric Observatory for Infrared Astronomy (SOFIA) to survey RCW 120 in the [CII] 1.9-THz fine-structure line of ionized carbon. These observations are part of the SOFIA FEEDBACK legacy program dedicated to study the interaction of massive stars with their environment (*30*). We have also used the Large APEX sub-Millimetre Array (LAsMA) instrument on the Atacama Pathfinder Experiment (APEX) to observe the J = 3-2 isotopologues of CO (see Materials and Methods).

The strongest [CII] emission toward RCW 120 is found in a limb-brightened ring surrounding the HII region, with lower integrated intensities toward the HII region interior (see Fig. 1). The [CII] emission is morphologically similar to the 8-μm emission, which is a reliable tracer of the photodissociation region (PDR), the interface between the fully ionized HII region, and the surrounding neutral and molecular gas. The ^{12}CO(3-2) and ^{13}CO(3-2) emission around RCW 120 is found in denser clumps and filaments compared to that of [CII]. Although we have not observed the northwestern quadrant of the region in [CII], our CO measurements indicate that the ring is open toward the north and shows evidence for punctures in several locations.

Kinematic analysis of the [CII] data reveals a blue-shifted shell, which is visible as a curved structure in position-velocity (p-v) diagrams (see Fig. 2). The morphology of the emission is roughly isotropic, consistent with that of a half-shell expanding toward us at ~15 km/s. Expansion signatures are absent in ^{12}CO(3-2) and ^{13}CO(3-2) emission. This implies that the C^+/C/CO transition lies in the ambient molecular cloud beyond the shell. We also detect faint, but widespread, [CII] emission from the bubble interior at the

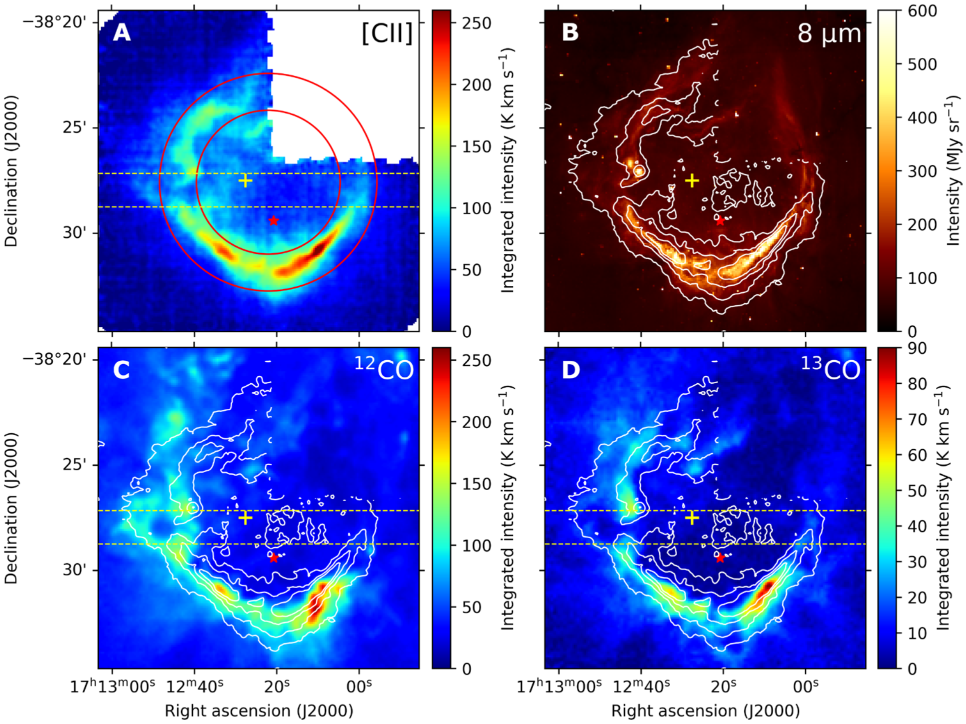

Fig. 1. Morphology of RCW 120 in different tracers. (**A**) SOFIA [CII] integrated intensity, scaled from 0 to 260 K km/s. The red circles indicate the approximate inner and outer PDR boundaries defined from Spitzer GLIMPSE 8-µm emission (*55*), and the red star shows the location of the ionizing source, CD −38°11636. The yellow "+" indicates "Position 1" (see the Supplementary Materials). (**B**) Spitzer GLIMPSE 8-µm emission. The contours are of [CII] integrated intensity, scaled from 40 to 160 K km/s in 40 K km/s increments. (**C** and **D**) APEX ^{12}CO(3-2) and ^{13}CO(3-2) integrated intensity, scaled from 0 to 260 K and 0 to 90 K km/s, respectively. The contours are the same as in (B). The areas enclosed by the dashed yellow lines in (A), (C), and (D) were used to extract the position-velocity diagrams shown in Fig. 2.

systemic velocity of the large-scale cloud [−7.5 km/s, as determined from the APEX CO(3-2) data and Mopra CO(1-0) data (*18*)] and also, at some positions, at positive (red-shifted) velocities. The red-shifted emission indicates expansion with a velocity of ~10 km/s away from us with respect to the systemic velocity of the cloud (see the Supplementary Materials). While this signature is blended with that of the systemic [CII] emission in the p-v diagrams, it is seen as a separate component in a number of individual spectra toward the region. The red-shifted shell is less massive and more clumpy than the blue-shifted shell and may reflect localized punctures through the molecular gas found at the backside of RCW 120.

Given the expansion velocity of the [CII] shell, we estimate the dynamical age of the region to be ~0.15 million years (Ma), lower than previous estimates (*15*, *20*), but roughly consistent with radiation-hydrodynamics simulations (*31*). The morphology of RCW 120 suggests that, with the exception of the background cloud at the systemic velocity, the entire shell is expanding at ~15 km/s.

Diffuse x-ray emission

The Chandra x-ray observatory has measured diffuse x-ray emission toward RCW 120, revealing the existence of hot (4×10^6 K) plasma created by the stellar wind from CD −38°11636 (*32*); see Fig. 3. Toward the dense southern shell, the hot plasma is confined to the interior of the bubble, but it has ruptured the shell toward the east and the north. [SII] observations show that the 10^4 K HII region gas is primarily found toward the edges of the region (*33*). We find a filling factor of ~0.2 for the HII region gas (see the Supplementary Materials), suggesting that the remaining ~80% of the bubble is filled with the hot x-ray plasma.

Stellar wind feedback and energetics

The picture that emerges from the wealth of our data reveals that the ~2500 km/s (*34*) wind from CD −38°11636 is shocked, creating a hot plasma that radiates in x-rays (Figs. 3 and 4). The overpressurized hot gas drives a strong shock wave, sweeping up the surrounding medium into a dense shell (*6*). This shell is ionized on the inside by extreme ultraviolet ($E > 13.6$ eV) photons, radiating in Hα and [SII] (*15*, *33*). The remainder of the shell consists of neutral gas in a PDR created by impinging far ultraviolet ($6 < E < 13.6$ eV) photons (*35*). The PDR is traced by the 8-µm emission of polycyclic aromatic hydrocarbon molecules and by its dominant cooling line, the [CII] 1.9 THz fine-structure line (*36*); see Fig. 1.

The total kinetic energy of the expanding shell is 1×10^{47} to 13×10^{47} erg, which is a considerable fraction of the mechanical luminosity of the stellar wind over the age of the bubble (15×10^{47} erg). By comparison, the thermal energies of the ionized gas and the hot x-ray plasma are 5×10^{46} and 17×10^{46} erg, respectively (see Table 1). The ratio of the kinetic energy of the swept up shell to the thermal energy of the hot plasma is possibly much larger (up to a factor of ~8) than predicted for adiabatic expansion of stellar wind bubbles of 1.2 (*6*). The thermal energy may be reduced because of the breach in the northeast, where hot plasma appears to be leaking out of the HII region. Hot gas is also flowing out through the northern opening of the shell (Fig. 1), which may have further reduced the

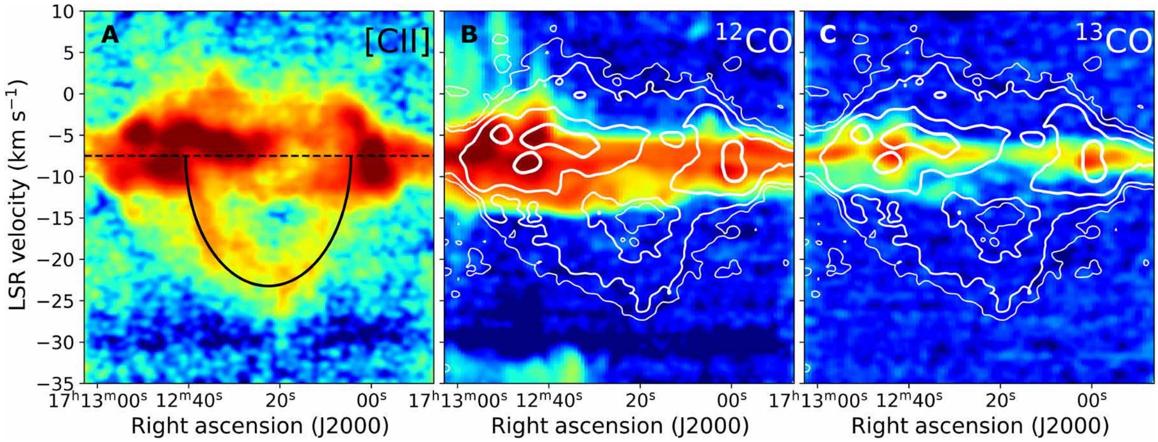

Fig. 2. Position-velocity (p-v) diagrams. (**A**) p-v diagram of the [CII] emission extracted from the area within the dashed yellow lines shown in Fig. 1A. The data were smoothed to a spatial resolution of 20″ and a velocity resolution of 0.8 km/s. The color scale is logarithmic and was chosen to highlight the blue-shifted, curved [CII] emission. The dashed black line shows the systemic [CII] velocity of the region and the black semi-ellipse shows our best-fit solution for the curve. The morphology of the blue-shifted emission reveals the presence of a [CII] shell expanding at ~15 km/s toward us. The red-shifted shell is not readily apparent in the p-v diagram as it is fainter and blended in with the bulk emission. (**B**) Same, for ^{12}CO(3-2) emission. The white contours are of the [CII] emission shown in (A). (**C**) Same, for ^{13}CO(3-2) emission. Expansion signatures are not seen in ^{12}CO and ^{13}CO.

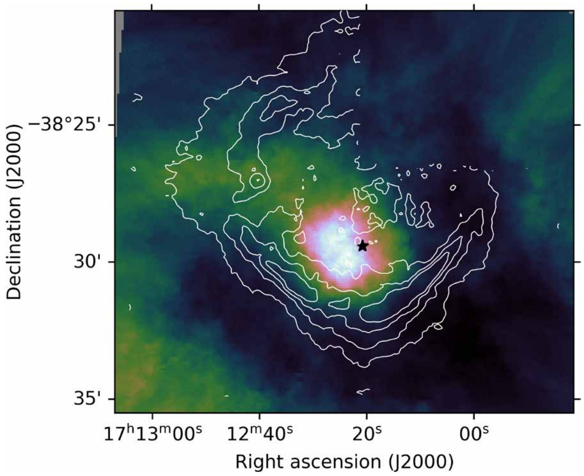

Fig. 3. Chandra diffuse x-ray emission toward RCW 120. The color scale ranges from 0 to 1.1×10^{-9} photons cm^{-2} s^{-1} arc sec^{-2}. The contours are of integrated [CII] intensity, scaled from 40 to 160 K km/s in 40 K km/s increments, and the location of the ionizing source is marked by the black star. There is strong diffuse x-ray emission within the bubble, which is breaching the PDR toward the northeast.

thermal energy of the plasma. The x-ray emission from the plasma in the north is likely obscured by a higher column density of neutral foreground gas. Furthermore, this ratio does not take into account electron conduction of the hot gas into the shell balanced by mass evaporation of shell gas into the hot gas and rapid radiative cooling in the mixing layer. This mass loading dissipates additional thermal energy, while simultaneously decreasing the pressure in the bubble. While the leaking hot gas may have stopped to inject energy into the expanding shell, the breaches in the northeast and north may have occurred recently enough that this would have only a small effect on the kinetic energy of the shell. We find a thermal pressure of 3×10^4 K cm^{-3} in the surrounding molecular cloud in which the shell is expanding, and a ram pressure from the stellar wind of 8×10^5 K cm^{-3}, which is similar to the measured thermal pressure of the hot x-ray plasma of 7×10^5 K cm^{-3}.

In a system in which the ionizing star is moving supersonically with respect to the ambient cloud, a bow shock forms ahead of the star. The open shell toward the north of RCW 120 and the offset of the star from the center of the bubble are reminiscent of bow shock models for ultracompact HII regions such as G29.96-0.02 (*27*, *37*–*40*). In these models, a "stationary" shell structure (in the rest frame of the star) develops rapidly at the standoff distance of the bow shock that channels the flow of the material around it. The hot plasma, confined by the shell, is forced to flow downstream, where it quickly punches through the shell. A detailed model developed specifically for RCW 120 (*27*) explains the observed morphology well for a <~4 km/s motion of the star in the plane of the sky, consistent with its estimated proper motion of 2 to 4 km/s (*22*).

However, the mass flow around the shell in this model is at variance with the velocity field revealed by our observations. These models suggest that convection of energy and mass across the contact discontinuity between the hot plasma and the photo-ionized inner shell gas leads to rapid cooling and, as the thermal energy added by the wind is quickly lost, the expansion stalls. At that point, the main flow of the neutral gas is along the shell walls. Given the observed rapid expansion, we conclude that these models overestimate the energy and mass transfer across this boundary possibly because energy conduction by electrons is greatly limited by the magnetic field (*41*). As argued below, however, substantial magnetic fields are unlikely in RCW 120, and this effect possibly does not play a role in this source. In addition, the structure of the boundary in the model is determined by numerical diffusion, rather than by physical processes such as thermal conduction (*27*). We also see little evidence for Kelvin-Helmholtz instabilities that could mix cold shell gas into the hot plasma. The 24-μm dust arc observed at a distance of 0.25 pc from the star indicates a smooth flow of the ionized gas from the (southern) ionization front into the bubble and then on toward the north (*27*, *42*).

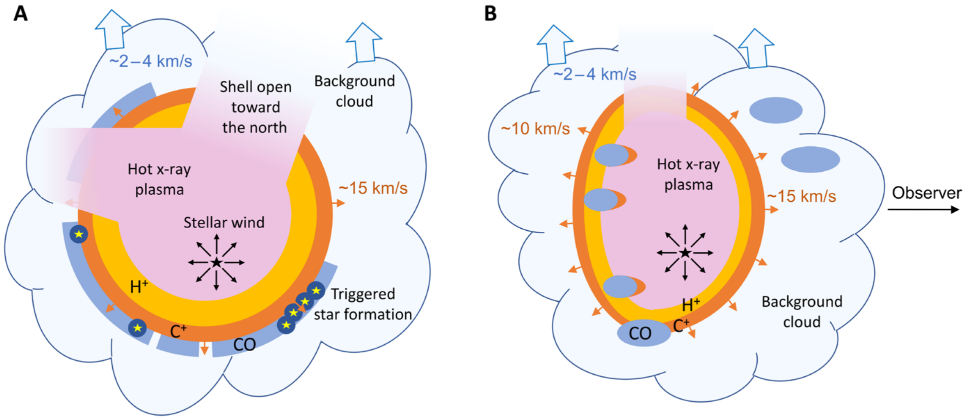

Fig. 4. Sketch of the structure of RCW 120. (**A**) Face-on view. The stellar wind from CD −38°11636 shocks the surrounding gas and creates a hot x-ray–emitting plasma. The energy injected by the stellar wind drives the rapid (~15 km/s) expansion of the [CII] shell. This expansion compresses the surrounding molecular gas and is responsible for the triggered star formation observed near the region edges. The shell is punctured toward the east and open toward the north, where the hot plasma is leaking into the surrounding medium. The surrounding large-scale molecular background cloud moves with a velocity of 2 to 4 km/s to the north with respect to the ionizing star (*22*, *27*). (**B**) Side view. The expansion of the shell toward its rear side is partially prevented by higher-pressure molecular gas structures. The systemic [CII] emission at a velocity of −7.5 km/s originates from these regions. The back side expands freely at several locations, giving rise to the red-shifted [CII] shell. Toward the front, the shell is expanding more homogeneously, suggesting that the foreground molecular gas is not strongly blocking the shell.

In addition, the morphology of the IR and x-ray observations reveal the presence of a puncture of the shell on the east side (Fig. 3). The surrounding cloud toward the rear side of the region has partially stopped the expansion of the shell in that direction. However, the [CII] velocity data suggest that the shell has also been punctured toward the rear side. This has allowed some of the x-ray emitting gas to flow out into the surrounding filamentary structure of the background cloud. The fact that these punctures predominantly occur toward the shell in the rear but not the front may be connected to instabilities caused by the interaction of the hot plasma within the bubble with the shell. There is no evidence that either the leakage or the surrounding cloud have stopped the expansion of the shell in any other direction. While traditional uniform background density models provide no explanation for such punctures, smoothed particle hydrodynamics models using an initial fractal density structure are able to reproduce perforations in the shell (*26*). This model, however, assumed that preexisting clumps are compressed by ionization erosion, for which we do not have evidence here. Further numerical simulations (see the Supplementary Materials) may help in determining the origin of these effects.

Triggered star formation

Morphologically, the star-forming CO clumps visible in Fig. 1 are part of the shell and are formed by compression in situ as preexisting clumps would be quickly left behind by the expanding shell inside the ionized gas/plasma bubble. Given the absence of pillars and globules in RCW 120, which are typically found in simulations with high fractal dimensions (*26*) and a high degree of turbulence (*43*), we believe that the initial molecular cloud was fairly homogeneous, making a substantial number of preexisting clumps unlikely. The densest clumps in the shell have already formed stars (see the Supplementary Materials). As a corollary, star formation must have proceeded very rapidly after shell formation. The shell expands supersonically into the background cloud, shocking the swept up gas at 15 km/s. The shocked gas will cool rapidly and that greatly increases the density. For a thin shell ($N_H < \sim 5 \times 10^{21}$ cm^{-2}), the [CII] fine-structure line will limit the cooling to about $T > \sim 100$ K in the PDR side facing the star, corresponding to a sound speed of >~1 km/s in the PDR. This implies a compression by a factor $(v_s/c_{PDR})^2$ of <~200 (where v_s is the speed of the shell and c_{PDR} is the sound speed in the PDR). For larger column densities, CO can form in the PDR, cooling the gas down to ~20 to 30 K. At 30 K, the sound speed is ~0.5 km/s, and the resulting compression is then a factor of ~1000. With a preshock density of ~10^3 cm^{-3} (see the Supplementary Materials), the clump density is estimated to be ~10^6 cm^{-3}. The fastest collapse time scale is the free-fall time scale, $t_{ff} = 0.06(10^6 \mathrm{cm}^{-3}/n)^{1/2}$ Ma. Assuming a lower preshock density of 10^2 cm^{-3}, the clump density would be 10^5 cm^{-3}, corresponding to a free-fall time of 0.2 Ma. With an estimated lifetime of ~0.15 Ma for the bubble, the shell itself has not had the time to collapse, but the densest CO clumps would have had enough time to form stars after being compressed by the expanding shell. Several of the densest clumps have already formed stars, particularly in the more highly compressed shell toward the south of the region.

The absence of an expansion signature in ^{12}CO(3-2) and ^{13}CO(3-2) emission is at first glance unexpected as simulations qualitatively suggest that gas is "pushed away" during the expansion of the HII region (*26*, *43*). Although this may appear intuitive, models show that the difference between the initial velocity of the cloud and that of formed clumps after being compressed by an expanding shell is small (on the order of one to a few kilometers per second) (*44*). For the CO structures in the backside of the HII region, the expansion would naturally be much slower than that of the [CII] shell due to the large density variations between the clump and interclump gas, whereas any motion of the dense, star-forming clumps in the southern ring would be perpendicular to the line of sight and therefore not detected spectrally. These results are consistent with the observed ^{12}CO(3-2) and ^{13}CO(3-2) velocity structure and that of clumps formed by cooling and compression in the expanding shell.

In a future study, we intend to discuss the origin scenario of RCW 120, to investigate the hypothesis that the region was formed by the collision of two molecular clouds (*21*). In this scenario, the

Table 1. Properties of the different components of RCW 120

Component	Mass ($M_\odot$)	Thermal energy (10^{46} erg)	Kinetic energy (10^{46} erg)	Luminosity ($L_\odot$)	Pressure (10^6 K cm^{-3})
Expanding [CII] shell	40–520*	0.1–1.3	10–120	-	1–10
Molecular gas	2500	2.1	-	-	0.015
Ionized gas	26†	5.1	-	-	8‡
Stellar wind§	-	-	150	80‖	0.8¶
Hot x-ray plasma	0.05	17	-	0.10	0.7
CD −38°11636	-	-	-	9.1×10^4	-
[CII]	-	-	-	690	-
^{12}CO(3-2)	-	-	-	2.6	-
^{13}CO(3-2)	-	-	-	0.58	-

*Total atomic mass. †From [SII] observations (*33*). ‡From (*20*). §Over the lifetime of the bubble. ‖Mechanical luminosity. ¶Dynamical pressure.

limb-brightened ring seen in the IR is interpreted as a cavity created by the cloud collision. Here, we emphasize that the CO data do not probe the expansion of the HII region but rather indicate the presence of two distinct clouds (see the Supplementary Materials). The observed morphology and velocity signature of the [CII] emission, however, reveal a relatively homogeneously expanding shell in RCW 120, making it unlikely that the shell structure itself was directly produced by the collision of two molecular clouds. This is very different from the study of the Infrared Dark Cloud G035.39-00.33, whose emission is interpreted in terms of colliding clouds (*45*). More work is required to fully understand the formation mechanism of RCW 120 in the context of the rapidly expanding shell seen in [CII].

The short lifetime of the bubble suggests that magnetic fields do not play a large role in its evolution. The high overpressure of the hot plasma and the ionized gas ensures that the global dynamics of the bubble are not affected by the magnetic field of the molecular cloud (*31*). If magnetic field strengths were substantial, the magnetic field would be frozen in the compressed shell and this would cushion the shock, limiting its compression efficiency (*46*). Models show that magnetic fields are, in general, preferentially oriented parallel to the expansion front (*31*, *47*). In this case, fragmentation would not be prevented, and the fragmentation time scale would be comparable to the free-fall time. Magnetically supercritical cores would be able to form and ambipolar diffusion, which typically works on time scales several times the free-fall time scale (*47*, *48*), may be minor. However, further gravitational collapse of fragments is likely to take longer due to the strong magnetic support. Further magnetohydrodynamic studies, including self-gravity, will be required to determine the influence of magnetic fields on the collapse of wind-driven shells.

We note that the Veil nebula in Orion—the shell driven by the stellar wind from θ^1 Ori C—shows no evidence for triggered star formation (*7*, *8*). This may reflect its limited column density and the absence of CO condensations (*49*). Alternatively, these differences may result from the presence of a substantial magnetic field in the Veil of $|B| > \sim 50\ \mu$G (*50*).

Half of all Galactic massive star formation regions create IR bubbles (*12*). If rapid expansion is a general characteristic of star-forming regions, our results have major ramifications for the study of galaxy formation in the early universe and their subsequent evolution. Little is known about the formation mechanisms of stars in the early universe. As the environment then was metal-poor, the stars are expected to have been massive and therefore would have produced strong feedback effects. Our observations suggest that rapid triggered star formation around these massive stars may have played an important role, possibly contributing to the large star formation densities observed in high-redshift galaxies (*51*). A broader survey of massive star formation regions in [CII] emission, as is currently undertaken in the SOFIA FEEDBACK legacy program (*30*), is required to understand the role of massive stars in the collection, compression, fragmentation, and collapse of molecular clouds.

MATERIALS AND METHODS

The [CII] line at 1.9 THz was observed with SOFIA on 10 June 2019 on a flight from Christchurch, New Zealand, using upGREAT (*52*). The map was split into four tiles (each covering an area of 7.26′ × 7.26′), of which three were observed. Each tile was mapped four times in total-power array-on-the-fly mode. The first two coverages were done once horizontally (along right ascension) and once vertically (along declination), with the array rotated by 19° on the sky. The second two coverages were shifted by 36″ to achieve the best possible coverage for the [OI] line (which was observed in parallel but is not discussed here). The final map is centered on Right Ascension (RA), Declination (Dec) [J2000] = $17^h12^m03.65^s$, −38°30′28.43″. A fast Fourier transform spectrometer with 4 GHz instantaneous bandwidth was used as the backend (*53*). The velocity resolution of the final data is 0.2 km/s. The intensity is given in units of main beam brightness (T_{MB}), assuming a forward efficiency, $\eta_f = 0.97$, and an average main beam efficiency of 0.65. The half-power beam width at 1.9 THz is 14.1″ and the final data have a pixel size of 5″. The root mean square (rms) main beam brightness is 1.8 K for 5″ pixels and 0.2 km/s velocity channels. The scientific objectives and technical details of the FEEDBACK program can be found at https://feedback.astro.umd.edu/ (*30*).

To improve the quality of the spectra, we identify systematic variations of the baseline originating in instabilities in the telescope system (namely from the backend, receiver, and telescope optics) and atmosphere over the course of the observations. During the calibration process, we produce an additional data product from the emission-free background source (OFF-source) measurements by subtracting subsequent OFF positions from each other. These "OFF-OFF" spectra are calibrated the same way as the "ON-OFF" spectra containing the astronomical information. The created set of spectra contains the dynamics of the telescope system and the atmosphere but no emission from the astronomical source. Subsequently, we identify features that account for most of the variance from the mean over the OFF-OFF spectra using principal component analysis (PCA). We do this individually for each of the 14 heterodyne pixels of the upGREAT low-frequency array (LFA) receiver and for each SOFIA flight where RCW 120 was observed. The PCA produces a set of components that describe the variance in the spectral structure over the course of the observations from which the baseline artifacts originate. We then reconstruct each ON-OFF spectrum containing information on the astronomical source in terms of these components via a linear combination. Here, a component is more strongly weighted the better the component describes the structure of the spectrum. Because the components are derived from a different set of observations than the ON-OFF spectra, only features characteristic to both sets of spectra will be included in this reconstruction. We lastly subtract each component from the ON-OFF spectrum. This process allows the removal of complex artificial features from a spectrum, which cannot be removed with a standard polynomial baseline fit.

RCW 120 was also mapped on 21 September 2019 in the ^{13}CO(3-2) and ^{12}CO(3-2) transitions at 330.6 and 345.8 GHz using the LAsMA array on the APEX telescope (*54*). LAsMA is a 7-pixel single polarization heterodyne array that allows simultaneous observations of the two isotopomers in the upper (^{12}CO) and lower (^{13}CO) sideband of the receiver, respectively. The array is arranged in a hexagonal configuration around a central pixel with a spacing of about two beam widths (θ_{mb} = 18.2″ at 345.8 GHz) between the pixels. The backends are advanced fast Fourier transform spectrometers (*53*) with a bandwidth of 2 × 4 GHz and a native spectral resolution of 61 kHz (0.053 km/s at 345 GHz). The mapping was done in total power on-the-fly mode using the same central position as the SOFIA [CII] map (RA, Dec [J2000] = $17^h12^m03.65^s$, −38°30′28.43″) and a clean reference position at RA, Dec [J2000] = $17^h10^m41^s$, −37°44′04″. The mapped region of 15′ × 15′ was split into four tiles. Each tile was scanned in both right ascension and declination with a spacing of 9.1″ (half the beam size) and oversampling to 6″ in scanning direction, resulting in a uniformly sampled map with high fidelity. The beam width at 345.8 GHz is 18.2″ and the final data cubes are gridded to a pixel size of 9.1″. The rms main beam temperature noise of the data is 0.5 K when resampled to 0.1 km/s in velocity.

SUPPLEMENTARY MATERIALS

Supplementary material for this article is available at http://advances.sciencemag.org/cgi/content/full/7/15/eabe9511/DC1

REFERENCES AND NOTES

1. J. P. Williams, C. F. McKee, The galactic distribution of OB associations in molecular clouds. *Astrophys. J.* **476**, 166–183 (1997).
2. P. F. Hopkins, E. Quataert, N. Murray, Stellar feedback in galaxies and the origin of galaxy-scale winds. *Mon. Not. R. Astron. Soc.* **421**, 3522–3537 (2012).
3. C.-G. Kim, E. C. Ostriker, W.-T. Kim, Three-dimensional hydrodynamic simulations of multiphase galactic disks with star formation feedback. I. Regulation of star formation rates. *Astrophys. J.* **776**, 1 (2013).
4. S. K. Walch, A. P. Whitworth, T. Bisbas, R. Wünsch, D. Hubber, Dispersal of molecular clouds by ionizing radiation. *Mon. Not. R. Astron. Soc.* **427**, 625–636 (2012).
5. J. I. Castor, D. C. Abbott, R. I. Klein, Radiation-driven winds in Of stars. *Astrophys. J.* **195**, 157–174 (1975).
6. R. Weaver, R. McCray, J. Castor, P. Shapiro, R. Moore, Interstellar bubbles. II. Structure and evolution. *Astrophys. J.* **218**, 377–395 (1977).
7. C. Pabst, R. Higgins, J. R. Goicoechea, D. Teyssier, O. Berne, E. Chambers, M. Wolfire, S. T. Suri, R. Guesten, J. Stutzki, U. U. Graf, C. Risacher, A. G. G. M. Tielens, Disruption of the Orion molecular core 1 by wind from the massive star θ^1 Orionis C. *Nature* **565**, 618–621 (2019).
8. C. Pabst, J. R. Goicoechea, D. Teyssier, O. Berné, R. D. Higgins, E. T. Chambers, S. Kabanovic, R. Güsten, J. Stutzki, A. G. G. M. Tielens, Expanding bubbles in Orion A: [C_{II}] observations of M 42, M 43, and NGC 1977. *Astron. Astrophys.* **639**, A2 (2020).
9. B. G. Elmegreen, C. J. Lada, Sequential formation of subgroups in OB associations. *Astrophys. J.* **214**, 725–741 (1977).
10. N. R. Walborn, J. Maíz-Apellániz, R. H. Barbá, Further insights into the structure of 30 Doradus from the *Hubble Space Telescope* instruments. *Astron. J.* **124**, 1601–1624 (2002).
11. E. Churchwell, M. S. Povich, D. Allen, M. G. Taylor, M. R. Meade, B. L. Babler, R. Indebetouw, C. Watson, B. A. Whitney, M. G. Wolfire, T. M. Bania, R. A. Benjamin, D. P. Clemens, M. Cohen, C. J. Cyganowski, J. M. Jackson, H. A. Kobulnicky, J. S. Mathis, E. P. Mercer, S. R. Stolovy, B. Uzpen, D. F. Watson, M. J. Wolff, The bubbling galactic disk. *Astrophys. J.* **649**, 759–778 (2006).
12. L. D. Anderson, T. M. Bania, D. S. Balser, V. Cunningham, T. V. Wenger, B. M. Johnstone, W. P. Armentrout, The *WISE* catalog of Galactic H II regions. *Astrophys. J. Suppl. Ser.* **212**, 1 (2014).
13. M. A. Kuhn, L. A. Hillenbrand, A. Sills, E. D. Feigelson, K. V. Getman, Kinematics in young star clusters and associations with *Gaia* DR2. *Astrophys. J.* **870**, 32 (2019).
14. Y. P. Georgelin, Y. M. Georgelin, Régions H II de l'hémisphére austral. *Astron. Astrophys. Sup.* **3**, 1 (1970).
15. A. Zavagno, M. Pomarès, L. Deharveng, T. Hosokawa, D. Russeil, J. Caplan, Triggered star formation on the borders of the Galactic H II region RCW 120. *Astron. Astrophys.* **472**, 835–846 (2007).
16. L. Deharveng, A. Zavagno, F. Schuller, J. Caplan, M. Pomarès, C. De Breuck, Star formation around RCW 120, the perfect bubble. *Astron. Astrophys.* **496**, 177–190 (2009).
17. A. Zavagno, D. Russeil, F. Motte, L. D. Anderson, L. Deharveng, J. A. Rodón, S. Bontemps, A. Abergel, J.-P. Baluteau, M. Sauvage, P. André, T. Hill, G. J. White, Star formation triggered by the Galactic H II region RCW 120. First results from the Herschel Space Observatory. *Astron. Astrophys.* **518**, L81 (2010).
18. L. D. Anderson, L. Deharveng, A. Zavagno, P. Tremblin, V. Lowe, M. R. Cunningham, P. Jones, A. M. Mullins, M. P. Redman, Mopra CO observations of the Bubble H II region RCW 120. *Astrophys. J.* **800**, 101 (2015).
19. M. Figueira, A. Zavagno, L. Deharveng, D. Russeil, L. D. Anderson, A. Men'shchikov, N. Schneider, T. Hill, F. Motte, P. Mège, G. LeLeu, H. Roussel, J.-P. Bernard, A. Traficante, D. Paradis, J. Tigè, P. Andrè, S. Bontemps, A. Abergel, Star formation towards the Galactic H II region RCW 120. Herschel observations of compact sources. *Astron. Astrophys.* **600**, A93 (2017).
20. M. Figueira, A. Zavagno, L. Bronfman, D. Russeil, R. Finger, F. Schuller, APEX CO observations towards the photodissociation region of RCW 120. *Astron. Astrophys.* **639**, A93 (2020).
21. K. Torii, K. Hasegawa, Y. Hattori, H. Sano, A. Ohama, H. Yamamoto, K. Tachihara, S. Soga, S. Shimizu, T. Okuda, N. Mizuno, T. Onishi, A. Mizuno, Y. Fukui, Cloud-cloud collision as a trigger of the high-mass star formation: A molecular line study in RCW120. *Astrophys. J.* **806**, 7 (2015).
22. K. A. Marsh, A. P. Whitworth, RCW 120: A possible case of hit and run, elucidated by multitemperature dust mapping. *Mon. Not. R. Astron. Soc.* **483**, 352–358 (2019).
23. M. S. Kirsanova, Y. N. Pavlyuchenkov, D. S. Wiebe, P. A. Boley, S. V. Salii, S. V. Kalenskii, A. M. Sobolev, L. D. Anderson, Molecular envelope around the HII region RCW 120. *Mon. Not. R. Astron. Soc.* **488**, 5641–5650 (2019).
24. A. Zavagno, P. Andrè, F. Schuller, N. Peretto, Y. Shimajiri, D. Arzoumanian, T. Csengeri, M. Figueira, G. A. Fuller, V. Könyves, A. Men'shchikov, P. Palmeirin, H. Roussel, D. Russeil, N. Schneider, S. Zhang, The role of Galactic H II regions in the formation of filaments. High-resolution submillimeter imaging of RCW 120 with ArTéMiS. *Astron. Astrophys.* **638**, A7 (2020).
25. P. Tremblin, N. Schneider, V. Minier, P. Didelon, T. Hill, L. D. Anderson, F. Motte, A. Zavagno, André, D. Arzoumanian, E. Audit, M. Benedettini, S. Bontemps, T. Csengeri, J. Di Francesco, T. Giannini, M. Hennemann, Q. N. Luong, A. P. Marston, N. Peretto, A. Rivera-Ingraham, D. Russeil, K. L. J. Rygl, L. Spinoglio, G. J. White, Ionization compression impact on dense gas distribution and star formation. Probability density functions around H II regions as seen by Herschel. *Astron. Astrophys.* **564**, A106 (2014).

26. S. Walch, A. P. Whitworth, T. G. Bisbas, D. A. Hubber, R. Wünsch, Comparing simulations of ionization triggered star formation and observations in RCW 120. *Mon. Not. R. Astron. Soc.* **452**, 2794–2803 (2015).
27. J. Mackey, V. V. Gvaramadze, S. Mohamed, N. Langer, Wind bubbles within H II regions around slowly moving stars. *Astron. Astrophys.* **573**, A10 (2015).
28. V. V. Akimkin, M. S. Kirsanova, Y. N. Pavlyuchenkov, D. S. Wiebe, Dust dynamics and evolution in H II regions—II. Effects of dynamical coupling between dust and gas. *Mon. Not. R. Astron. Soc.* **469**, 630–638 (2017).
29. A. Rodríguez-González, Z. Meliani, M. Sánchez-Cruces, P. R. Rivera-Ortiz, A. Castellanos-Ramírez, Numerical models for the dust in RCW 120. *Astron. Astrophys.* **631**, A170 (2019).
30. N. Schneider, R. Simon, C. Guevara, C. Buchbender, R. D. Higgins, Y. Okada, J. Stutzki, R. Güsten, L. D. Anderson, J. Bally, H. Beuther, L. Bonne, S. Bontemps, E. Chambers, T. Csengeri, U. U. Graf, A. Gusdorf, K. Jacobs, M. Justen, S. Kabanovic, R. Karim, M. Luisi, K. Menten, M. Mertens, B. Mookerjea, V. Ossenkopf-Okada, C. Pabst, M. W. Pound, H. Richter, N. Reyes, O. Ricken, M. Röllig, D. Russeil, Á. Sánchez-Monge, G. Sandell, M. Tiwari, H. Wiesemeyer, M. Wolfire, F. Wyrowski, A. Zavagno, A. G. G. M. Tielens, FEEDBACK: A SOFIA legacy program to study stellar feedback in regions of massive star formation. *Publ. Astron. Soc. Pac.* **132**, 104301 (2020).
31. S. J. Arthur, W. J. Henney, G. Mellema, F. de Colle, E. Vázquez-Semadeni, Radiation-magnetohydrodynamic simulations of H II regions and their associated PDRs in turbulent molecular clouds. *Mon. Not. R. Astron. Soc.* **414**, 1747–1768 (2011).
32. L. K. Townsley, P. S. Broos, G. P. Garmire, G. E. Anderson, E. D. Feigelson, T. Naylor, M. S. Povich, The massive star-forming regions omnibus x-ray catalog, second installment. *Astrophys. J. Suppl. S.* **235**, 43 (2018).
33. M. Sánchez-Cruces, A. Castellanos-Ramírez, M. Rosado, A. Rodríguez-González, J. Reyes-Iturbide, Kinematics of the galactic bubble RCW 120. *Rev. Mex. Astron. Astr.* **54**, 375–388 (2018).
34. J. Puls, N. Markova, S. Scuderi, C. Stanghellini, O. G. Taranova, A. W. Burnley, I. D. Howarth, Bright OB stars in the Galaxy. III. Constraints on the radial stratification of the clumping factor in hot star winds from a combined H_α, IR and radio analysis. *Astron. Astrophys.* **454**, 625–651 (2006).
35. D. J. Hollenbach, A. G. G. M. Tielens, Photodissociation regions in the interstellar medium of galaxies. *Rev. Mod. Phys.* **71**, 173–230 (1999).
36. A. G. G. M. Tielens, *The Physics and Chemistry of the Interstellar Medium* (Cambridge Univ. Press, 2010).
37. G. Tenorio-Tagle, The gas dynamics of H II regions. I. The champagne model. *Astron. Astrophys.* **71**, 59–65 (1979).
38. M.-M. Mac Low, D. van Buren, D. O. S. Wood, E. Churchwell, Bow shock models of Ultracompact H II Regions. *Astrophys. J.* **369**, 395 (1991).
39. S. J. Arthur, M. G. Hoare, Hydrodynamics of Cometary Compact H II Regions. *Astrophys. J. Suppl. S.* **165**, 283–306 (2006).
40. S. Verdolini, S. C. C. Yeh, M. R. Krumholz, C. D. Matzner, A. G. G. M. Tielens, Line emission from radiation-pressurized H II Regions. II. Dynamics and population synthesis. *Astrophys. J.* **769**, 12 (2013).
41. L. L. Cowie, C. F. McKee, The evaporation of spherical clouds in a hot gas. I. Classical and saturated mass loss rates. *Astrophys. J.* **211**, 135–146 (1977).
42. B. B. Ochsendorf, S. Verdolini, N. L. J. Cox, O. Berné, L. Kaper, A. G. G. M. Tielens, Radiation-pressure-driven dust waves inside bursting interstellar bubbles. *Astron. Astrophys.* **566**, A75 (2014).
43. P. Tremblin, E. Audit, V. Minier, W. Schmidt, N. Schneider, Three-dimensional simulations of globule and pillar formation around HII regions: Turbulence and shock curvature. *Astron. Astrophys.* **546**, A33 (2012).
44. M. Gritschneder, A. Burkert, T. Naab, S. Walch, Detailed numerical simulations on the formation of pillars around H II Regions. *Astrophys. J.* **723**, 971–984 (2010).
45. T. G. Bisbas, J. C. Tan, T. Csengeri, B. Wu, W. Lim, P. Caselli, R. Güsten, O. Ricken, D. Riquelme, The inception of star cluster formation revealed by [C II] emission around an infrared dark cloud. *Mon. Not. R. Astron. Soc.* **478**, L54–L59 (2018).
46. D. Hollenbach, C. F. McKee, Molecule formation and infrared emission in fast interstellar shocks. III. Results for J shocks in molecular clouds. *Astrophys. J.* **342**, 306 (1989).
47. F. Heitsch, L. Hartmann, Accretion and diffusion time-scales in sheets and filaments. *Mon. Not. R. Astron. Soc.* **443**, 230–240 (2014).
48. L. Mestel, L. Spitzer Jr., Star formation in magnetic dust clouds. *Mon. Not. R. Astron. Soc.* **116**, 503–514 (1956).
49. J. R. Goicoechea, C. H. M. Pabst, S. Kabanovic, M. G. Santa-Maria, N. Marcelino, A. G. G. M. Tielens, A. Hacar, O. Berné, C. Buchbender, S. Cuadrado, R. Higgins, C. Kramer, J. Stutzki, S. Suri, D. Teyssier, M. Wolfire, Molecular globules in the Veil bubble of Orion. IRAM 30 m ^{12}CO, ^{13}CO, and C^{18}O (2-1) expanded maps of Orion A (2020). *Astron. Astrophys.* **639**, A1 (2020).
50. T. H. Troland, W. M. Goss, C. L. Brogan, R. M. Crutcher, D. A. Roberts, Orion's Veil: Magnetic field strengths and other properties of a PDR in front of the trapezium cluster. *Astrophys. J.* **825**, 2 (2016).
51. P. Madau, M. Dickinson, Cosmic star-formation history. *Annu. Rev. Astron. Astrophys.* **52**, 415–486 (2014).
52. C. Risacher, R. Güsten, J. Stutzki, H.-W. Hübers, R. Aladro, A. Bell, C. Buchbender, D. Büchel, T. Csengeri, C. Duran, U. U. Graf, R. D. Higgins, C. E. Honingh, K. Jacobs, M. Justen, B. Klein, M. Mertens, Y. Okada, A. Parikka, P. Pütz, N. Reyes, H. Richter, O. Ricken, D. Riquelme, N. Rothbart, N. Schneider, R. Simon, M. Wienold, H. Wiesemeyer, M. Ziebart, P. Fusco, S. Rosner, B. Wohler, The upGREAT dual frequency heterodyne arrays for SOFIA. *J. Astron. Instrum.* **7**, 1840014 (2018).
53. B. Klein, S. Hochgürtel, I. Krämer, A. Bell, K. Meyer, R. Güsten, High-resolution wide-band fast Fourier transform spectrometers. *Astron. Astrophys.* **542**, L3 (2012).
54. R. Güsten, L. Å. Nyman, P. Schilke, K. Menten, C. Cesarsky, R. Booth, The Atacama Pathfinder EXperiment (APEX)—A new submillimeter facility for southern skies. *Astron. Astrophys.* **454**, L13–L16 (2006).
55. R. A. Benjamin, E. Churchwell, B. L. Babler, T. M. Bania, D. P. Clemens, M. Cohen, J. M. Dickey, R. Indebetouw, J. M. Jackson, H. A. Kobulnicky, A. Lazarian, A. P. Marston, J. S. Mathis, M. R. Meade, S. Seager, S. R. Stolovy, C. Watson, B. A. Whitney, M. J. Wolff, M. G. Wolfire, GLIMPSE. I. An *SIRTF* legacy project to map the inner galaxy. *Publ. Astron. Soc. Pac.* **115**, 953–964 (2003).
56. L. D. Anderson, T. M. Bania, J. M. Jackson, D. P. Clemens, M. Heyer, R. Simon, R. Y. Shah, J. M. Rathborne, The molecular properties of galactic H II regions. *Astrophys. J. Suppl. S.* **181**, 255–271 (2009).
57. L. D. Anderson, T. M. Bania, D. S. Balser, R. T. Rood, The Green Bank Telescope H II region discovery survey. II. The source catalog. *Astrophys. J. Suppl. S.* **194**, 32 (2011).
58. M. Figueira, L. Bronfman, A. Zavagno, F. Louvet, N. Lo, R. Finger, J. Rodón, ALMA observations of RCW 120 fragmentation at 0.01 pc scale. *Astron. Astrophys.* **616**, L10 (2018).
59. F. Martins, M. Pomarès, L. Deharveng, A. Zavagno, J. C. Bouret, Near-IR integral field spectroscopy of ionizing stars and young stellar objects on the borders of H II regions. *Astron. Astrophys.* **510**, A32 (2010).
60. C. Guevara, J. Stutzki, V. Ossenkopf-Okada, R. Simon, J. P. Pérez-Beaupuits, H. Beuther, S. Bihr, R. Higgins, U. Graf, R. Güsten, [C II] 158 μm self-absorption and optical depth effects. *Astron. Astrophys.* **636**, A16 (2020).
61. T. Robitaille, T. Rice, C. Beaumont, A. Ginsburg, B. MacDonald, E. Rosolowski, astrodendro: Astronomical data dendrogram creator. *Astrophysics Source Code Library*, ascl:1907.016 (2019).
62. S. N. Milam, C. Savage, M. A. Brewster, L. M. Ziurys, S. Wyckoff, The ^{12}C/^{13}C isotope gradient derived from millimeter transitions of CN: The case for galactic chemical evolution. *Astrophys. J.* **634**, 1126–1132 (2005).
63. U. J. Sofia, J. T. Lauroesch, D. M. Meyer, S. I. B. Cartledge, Interstellar carbon in translucent sight lines. *Astrophys. J.* **605**, 272–277 (2004).
64. M. Riener, J. Kainulainen, J. D. Henshaw, J. H. Orkisz, C. E. Murray, H. Beuther, GAUSSPY+: A fully automated Gaussian decomposition package for emission line spectra. *Astron. Astrophys.* **628**, A78 (2019).
65. J. Mangum, Y. Shirley, How to calculate molecular column density. *Publ. Astron. Soc. Pac.* **127**, 266–298 (2015).
66. M. Tiwari, K. M. Menten, F. Wyrowski, J. P. Pérez-Beaupuits, H. Wiesemeyer, R. Güsten, B. Klein, C. Henkel, Unveiling the remarkable photodissociation region of Messier 8. *Astron. Astrophys.* **615**, A158 (2018).
67. L. D. Anderson, A. Zavagno, L. Deharveng, A. Abergel, F. Motte, P. André, J.-P. Bernard, S. Bontemps, M. Hennemann, T. Hill, J. A. Rodón, H. Roussel, D. Russeil, The dust properties of bubble H II regions as seen by Herschel. *Astron. Astrophys.* **542**, A10 (2012).
68. N. M. McClure-Griffiths, J. M. Dickey, B. M. Gaensler, A. J. Green, M. Haverkorn, S. Strasser, The southern galactic plane survey: H I observations and analysis. *Astrophys. J. Suppl. S.* **158**, 178–187 (2005).
69. D. S. Balser, T. V. Wenger, L. D. Anderson, T. M. Bania, Azimuthal metallicity structure in the milky way disk. *Astrophys. J.* **806**, 199 (2015).
70. J. S. Vink, A. de Koter, H. J. G. L. M. Lamers, New theoretical mass-loss rates of O and B stars. *Astron. Astrophys.* **362**, 295–309 (2000).
71. F. Martins, D. Schaerer, D. J. Hillier, A new calibration of stellar parameters of Galactic O stars. *Astron. Astrophys.* **436**, 1049–1065 (2005).
72. R. Simon, N. Schneider, J. Stutzki, R. Güsten, U. U. Graf, P. Hartogh, X. Guan, J. G. Staguhn, D. J. Benford, SOFIA observations of S106: Dynamics of the warm gas. *Astron. Astrophys.* **542**, L12 (2012).
73. C. Pabst, J. R. Goicoechea, D. Teyssier, O. Berné, B. B. Ochsendorf, M. G. Wolfire, R. D. Higgins, D. Riquelme, C. Risacher, J. Pety, F. Le Petit, E. Roueff, E. Bron, A. G. G. M. Tielens, [C II] emission from L1630 in the Orion B molecular cloud. *Astron. Astrophys.* **606**, A29 (2017).

74. N. Schneider, M. Röllig, R. Simon, H. Wiesemeyer, A. Gusdorf, J. Stutzki, R. Güsten, S. Bontemps, F. Comerón, T. Csengeri, J. D. Adams, H. Richter, Anatomy of the massive star-forming region S106. The [O I] 63 μm line observed with GREAT/SOFIA as a versatile diagnostic tool for the evolution of massive stars. *Astron. Astrophys.* **617**, A45 (2018).
75. G. J. Ferland, M. Chatzikos, F. Guzmán, M. L. Lykins, P. A. M. van Hoof, R. J. R. Williams, N. P. Abel, N. R. Badnell, F. P. Keenan, R. L. Porter, P. C. Stancil, The 2017 Release Cloudy. *Rev. Mex. Astron. Astr.* **53**, 385–438 (2017).
76. J. Stutzki, R. Güsten, High-spatial resolution isotopic CO and CS observations of M17 SW: The clumpy structure of the molecular cloud core. *Astrophys. J.* **356**, 513–533 (1990).
77. C. Kramer, J. Stutzki, R. Rohrig, U. Corneliussen, Clump mass spectra of molecular clouds. *Astron. Astrophys.* **329**, 249–264 (1998).
78. N. Schneider, J. Stutzki, G. Winnewisser, D. Block, The Rosette molecular complex. I. CO observations. *Astron. Astrophys.* **335**, 1049–1069 (1998).
79. F. Bertoldi, C. F. McKee, Pressure-confined clumps in magnetized molecular clouds. *Astrophys. J.* **395**, 140 (1992).
80. R. Simon, J. M. Jackson, D. P. Clemens, T. M. Bania, M. H. Heyer, The structure of four molecular cloud complexes in the BU-FCRAO milky way galactic ring survey. *Astrophys. J.* **551**, 747–763 (2001).
81. M. Röllig, V. Ossenkopf, S. Jeyakumar, J. Stutzki, A. Sternberg, [CII] 158 μm emission and metallicity in photon dominated regions. *Astron. Astrophys.* **451**, 917–924 (2006).
82. M. Röllig, R. Szczerba, V. Ossenkopf, C. Glück, Full SED fitting with the KOSMA-τ PDR code. I. Dust modelling. *Astron. Astrophys.* **549**, A85 (2013).
83. Q. A. Parker, S. Phillipps, M. J. Pierce, M. Hartley, N. C. Hambly, M. A. Read, H. T. MacGillivray, S. B. Tritton, C. P. Cass, R. D. Cannon, M. Cohen, J. E. Drew, D. J. Frew, E. Hopewell, S. Mader, D. F. Malin, M. R. W. Masheder, D. H. Morgan, R. A. H. Morris, D. Russeil, K. S. Russell, R. N. F. Walker, The AAO/UKST SuperCOSMOS Hα survey. *Mon. Not. R. Astron. Soc.* **362**, 689–710 (2005).

Acknowledgments: This study was based on observations made with the NASA/DLR Stratospheric Observatory for Infrared Astronomy (SOFIA). SOFIA is jointly operated by the Universities Space Research Association Inc. (USRA), under NASA contract NAS2-97001, and the Deutsches SOFIA Institut (DSI), under DLR contract 50 OK 0901 to the University of Stuttgart. upGREAT is a development by the MPI für Radioastronomie and the KOSMA/Universität zu Köln, in cooperation with the DLR Institut für Optische Sensorsysteme. APEX is a collaboration between the Max-Planck-Institut für Radioastronomie, Onsala Space Observatory (OSO), and the European Southern Observatory (ESO). We thank M. Sánchez-Cruces for helpful review of the [SII] observations of RCW 120. **Funding:** We acknowledge funding by the Bundesministerium für Wirtschaft und Energie through the grant FEEDBACK (50OR1916). N.S. and R.S. acknowledge support from the ANR and DFG grant "GENESIS" (ANR-16-CE92-0035-01/DFG1591/2-1). The GREAT team members of the I. Physik. Institut, University of Cologne, and Max-Planck Institut für Radioastronomie, Bonn, acknowledge funding from the DFG, project number SFB 956, projects A4, D2, and D3. L.D.A. acknowledges support from NSF grant AST1516021. A.Z. thanks the support from the Institut Universitaire de France. Financial support for the SOFIA Legacy Program, FEEDBACK, at the University of Maryland was provided by NASA through award SOF070077 issued by USRA. **Author contributions:** A.G.G.M.T. and N.S. conceived the FEEDBACK legacy survey, which motivated this study. M.L. and A.G.G.M.T. wrote the manuscript with input from all other authors. M.L. analyzed the data and generated the figures under L.D.A.'s guidance. R.S., C.B., J.S., K.J., M.J., and B.K. generated and processed the SOFIA [CII] observations. R.G. generated and processed the APEX CO observations. S.K., N.S., A.G.G.M.T., L.D.A., R.S., M.R., C.G., D.L., M.T., A.Z., and D.R. assisted on the analysis and interpretation of the [CII] and CO data. L.K.T. and P.S.B. analyzed and interpreted the Chandra x-ray data. All authors discussed the results. **Competing interests:** The authors declare that they have no competing interests. **Data materials and availability:** The [CII] data used in this study are publicly available in the SOFIA Science Archive at IRSA (https://irsa.ipac.caltech.edu/). All data needed to evaluate the conclusions in the paper are present in the paper and/or the Supplementary Materials.

Submitted 24 September 2020
Accepted 19 February 2021
Published 9 April 2021
10.1126/sciadv.abe9511

Citation: M. Luisi, L. D. Anderson, N. Schneider, R. Simon, S. Kabanovic, R. Güsten, A. Zavagno, P. S. Broos, C. Buchbender, C. Guevara, K. Jacobs, M. Justen, B. Klein, D. Linville, M. Röllig, D. Russeil, J. Stutzki, M. Tiwari, L. K. Townsley, A. G. G. M. Tielens, Stellar feedback and triggered star formation in the prototypical bubble RCW 120. *Sci. Adv.* **7**, eabe9511 (2021).

Science Advances

Stellar feedback and triggered star formation in the prototypical bubble RCW 120

Matteo LuisiLoren D. AndersonNicola SchneiderRobert SimonSlawa KabanovicRolf GüstenAnnie ZavagnoPatrick S. BroosChristof BuchbenderCristian GuevaraKarl JacobsMatthias JustenBernd KleinDylan LinvilleMarkus RölligDelphine RusseilJürgen StutzkiMaitraiyee TiwariLeisa K. TownsleyAlexander G. G. M. Tielens

Sci. Adv., 7 (15), eabe9511. • DOI: 10.1126/sciadv.abe9511

Science Advances (ISSN 2375-2548) is published by the American Association for the Advancement of Science. 1200 New York Avenue NW, Washington, DC 20005. The title *Science Advances* is a registered trademark of AAAS.